PHOTODISINTEGRATION OF He^3

A. T. VARFOLOMEEV and A. N. GORBUNOV

P. N. Lebedev Physics Institute, Academy of Sciences, U.S.S.R.

Submitted to JETP editor January 25, 1964

J. Exptl. Theoret. Phys. (U.S.S.R.) **47**, 30-39 (July, 1964)

The photodisintegration of He^3 was investigated with a cloud chamber in a magnetic field at maximum bremsstrahlung energy E_{max} = 170 MeV. In sharp contradiction to the theory which neglects the interaction of particles in the final state, the ratio of the two-particle to three-particle disintegration yields for He^3 was found to be unity. The cross section for two-particle disintegration is found to have a broad maximum at 12—13 MeV; its maximum value is ~1 mb. The integrated cross section is 26.5 ± 1.3 MeV-mb. The integrated bremsstrahlung-weighted cross section for photoabsorption by the He^3 nucleus is 2.68 ± 0.1 mb. The He^3 rms nuclear charge radius for point nucleons is 1.60 ± 0.07 F. When the finite proton size is taken into account the rms charge radius is 1.79 ± 0.07 F, in satisfactory agreement with results obtained from the experimental scattering of high-energy electrons. The c.m.s. proton angular distribution is closely represented by (5).

1. INTRODUCTION

IT is of interest to study the photodisintegration of the three-particle nuclei H^3 and He^3 as a means of determining to what extent nuclear forces in complex nuclei can be reduced to two-body interactions. The measurement of the cross sections for photodisintegration processes in these nuclei and a comparison with theoretical results based on different hypotheses regarding nuclear forces and wave functions provide a good test of the hypotheses. From the cross sections for photonuclear reactions in three-particle nuclei we obtain the cross section for photon absorption by these nuclei, $\sigma_{abs}(w)$. By comparing the integrated cross sections

$$\sigma_0 = \int \sigma_{abs}(w)\,dw \quad \text{and} \quad \sigma_{-1} = \int \sigma_{abs}(w)\frac{dw}{w}$$

with calculations of the same cross sections based on sum rules we can arrive at some conclusions regarding the role of exchange forces in nuclear interactions, and also obtain information about nuclear size. The rms radius of nuclear charge distribution serves as a good test of the parameters chosen for the wave functions used to describe the nuclear ground state.

Since there was very limited experimental information available regarding the photoeffect in three-particle nuclei[1], or regarding the inverse reactions,[2,3] we undertook a systematic investigation of the photodisintegration of He^3 in a cloud chamber.[1)]

2. EXPERIMENTAL PROCEDURE

A cloud chamber filled with He^3 to 0.9 atm gauge pressure and placed within a magnetic field of 10,400 Oe was operated in a bremsstrahlung beam having 170 MeV maximum energy. The He^3 was of better than 99.99% chemical purity; the tritium concentration did not exceed 10^{-11}%. The intensity of the radiation pulses registered by the cloud chamber was measured with a pulse ionization chamber calibrated in two different ways—by means of a quantameter[5] and by the yield from the reaction $C^{12}(\gamma, n)C^{11}$.[6] Discrepancies between the two calibrations did not exceed 3%. The magnetic field was measured with ~0.5% accuracy using a fluxmeter calibrated by nuclear resonance. The magnet current was stabilized within 0.05%. The present paper presents the results obtained from 22,300 stereoscopic cloud chamber photographs.

At energies below the meson threshold only two photonuclear reactions are possible in He^3:

$$He^3(\gamma, p)D^2 \text{ — two-particle disintegration,} \quad (1)$$

$$He^3(\gamma, n)2p \text{ — three-particle disintegration.} \quad (2)$$

[1)] Preliminary results have been published in[4].

FIG. 1. Cloud chamber photograph. a – the reaction $He^3(\gamma, p)D^2$ (the thin track belongs to a proton, and the denser track to a deuteron); b – the reaction $He^3(n, p)H^3$. The γ-ray beam was directed downward.

Typical photographs of these cases are shown in Figs. 1 and 2.

Our identification of the reactions (1) and (2) in the cloud chamber photographs was based on the conservation laws. Since two particles (a proton and a deuteron) appear in the final state, reaction (1) has the following characteristics: 1) in the c.m. system the two particles are emitted in opposite directions with equal momenta; 2) in the lab. system the two particles acquire a small amount of forward directivity, so that the vertex of the angle between the tracks points in the direction opposite to that of the beam, its magnitude being between $\sim 170°$ and 180°, depending on the directions of the particles; 3) the two tracks are coplanar with the axis of the γ beam; 4) the ionization density along the deuteron track is four times greater, on the average, than the ionization density along the proton track, since the proton and deuteron momenta are also approximately equal in the lab. system. In the final state of (2) three particles appear, of which only the two protons are registered in the cloud chamber. Therefore the proton tracks in this reaction can be oriented arbitrarily both with respect to each other and with respect to the direction of the γ beam.

The foregoing kinematic characteristics of reactions (1) and (2) allowed, in the very great majority of cases, a unique identification of these processes by means of visual scanning. In the relatively small number of events when the visual identification of (1) was doubtful we analyzed the disintegration kinematics quantitatively.

Some uncertainty in the identity of reaction (2) arose whenever one of the protons was stopped by the cloud chamber gas after a range of less than 10 mm. In such instances the short proton track can be mistaken for the track of a recoil nucleus in reactions such as

$$X + \gamma \rightarrow X' + p + n, \tag{3}$$

$$X + \gamma \rightarrow X'' + p \tag{4}$$

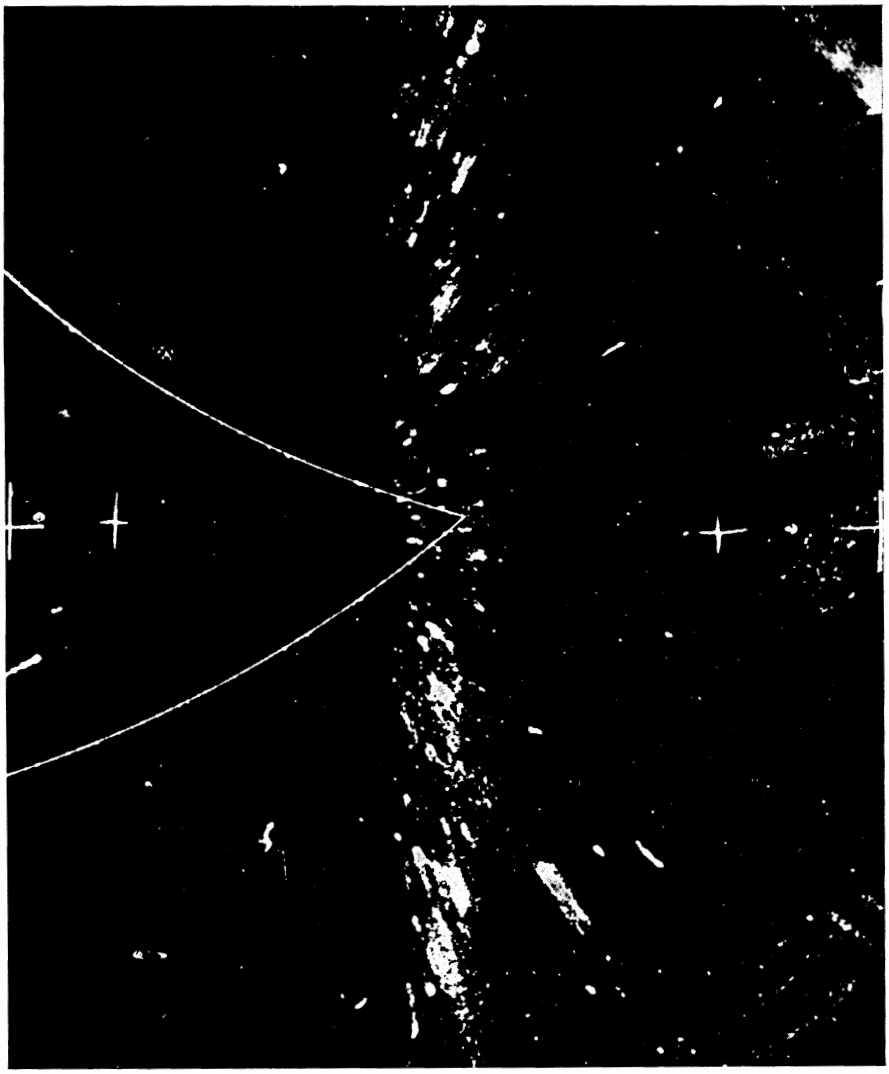

FIG. 2. An example of He^3 (γ, n)2p photographed in a cloud chamber.

involving carbon or oxygen nuclei contained in water or alcohol vapor. On the other hand, some instances of (3) and (4) could sometimes be assigned to (2). However, the number of such doubtful events was small. Moreover, the expected number of reactions (3) and (4) on impurities was easily computed from the observed yield of stars having more than two charged particles that were identified with certainty, and from the relative yields of different photonuclear reactions on carbon[7] and oxygen.[8] In this way a 2.5% correction of the number of events (2) was obtained.

In addition to reactions (1)—(4) each photograph revealed on the average one instance of the reaction $He^3(n,p)H^3$, very probably induced by slow neutrons. However, 99% of these events occurred outside the γ beam. Also, the external features of the reaction are so characteristic that it can be identified practically uniquely.

The emission angles of the particles were measured by reprojection, which provided us with a spatial picture of the event. The radii of curvature of tracks in the magnetic field were determined by comparison with standard circles. To insure sufficient accuracy of the measurements, we selected only those disintegrations where each of the two charged-particle tracks was inclined not more than 30° to the plane of the cloud chamber. A geometric correction was introduced in order to determine the total number of disintegrations with the appropriate kinematic characteristics. The energies of photons inducing disintegrations were determined from energy and momentum conservation.

The measurement errors were evaluated as follows. In reaction (1) the c.m.s. proton and deuteron momenta, p_1 and p_2, must be identical, and the sum of the angles θ_1 and θ_2 between the γ beam and the respective directions of p_1 and p_2 must be 180°. We characterized the measurement errors by the values of the ratio $\Delta p/(p_1 + p_2)$, where $\Delta p = |p_1 - p_2|$, and $\Delta\theta = |\theta_1 + \theta_2 - 180°|$. Figure 3 shows the experimental distributions of these char-

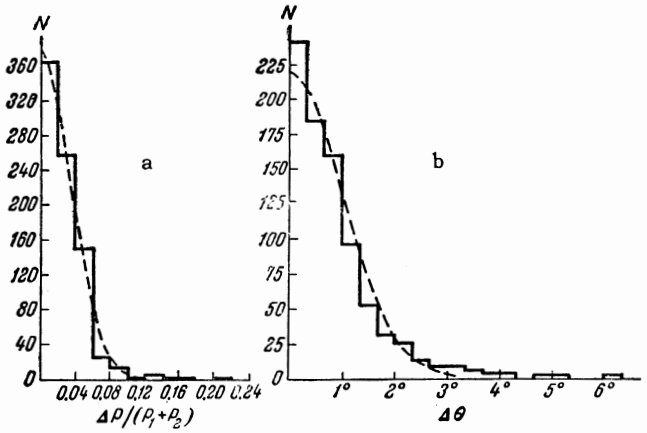

FIG. 3. Distribution of measurement errors. a – particle momenta; b – particle angle relative to the γ beam.

acteristics for 830 events of type (1). Both distributions are Gaussian with $\sigma = 0.035$ and 1°, respectively. The accordingly calculated error in determining the energy of γ rays from reaction (1) varies from 3% at 8 MeV to 9% at ~ 100 MeV. All numerical calculations were performed on an M-20 electronic computer.

3. EXPERIMENTAL RESULTS

A. Yields of $He^3(\gamma, p)D^2$ and $He^3(\gamma, n)2p$. In the 22,300 cloud chamber photographs we observed 2771 instances of (1) and 2780 instances of (2). It is thus shown that the yields of the (γ, p) and (γ, n) reactions on He^3 are equal within statistical error limits. The absolute yield of each of these reactions is

$$Y_1 = Y_2 = \int_0^{170} \sigma(w)\,\eta(w)\,dw = 1.47 \pm 0.03 \text{ mb},$$

where $\sigma(w)$ is the cross section for (1) or (2), and $\eta(w)$ is the bremsstrahlung spectrum. (We used the spectrum in [9].) An error of 5.5% was associated with the intensity measurements.

Our result differs sharply from the predictions of the theory of Gunn and Irving,[10] who assumed that nuclear forces can be represented by a two-body central Yukawa potential and that the particles do not interact in the final state. The theoretical cross section for the three-particle photodisintegration of He^3 [reaction (2)] should be about five times larger than the cross section for two-particle disintegration [reaction (1)].

B. Effective cross section for $He^3(\gamma, p)D^2$. The cross section for reaction (1) was determined from measurements of 830 events observed in a central region of the chamber 18 cm long, where the inclination of the tracks to the plane of the chamber did not exceed 30°. Since only two particles are produced in reaction (1), in order to determine the energy of the photon inducing the reaction it is sufficient to measure the emission angle and momentum of one of the particles (the proton or the deuteron). As a control, we measured the angles and momenta of both particles, and thus obtained a double determination of the photon energy. The cross sections obtained from the proton and deuteron tracks are given separately in Fig. 4. The mean cross section in each of the selected energy intervals is shown by the histogram in Fig. 4. For convenience in making the subsequent comparison with theoretical calculations, the histogram is approximated by a smooth curve. Figure 4 shows that the cross section for (1) has a broad peak at the photon energy ~ 12–13 MeV, with $\sigma_{max} \sim 1.0$ mb.

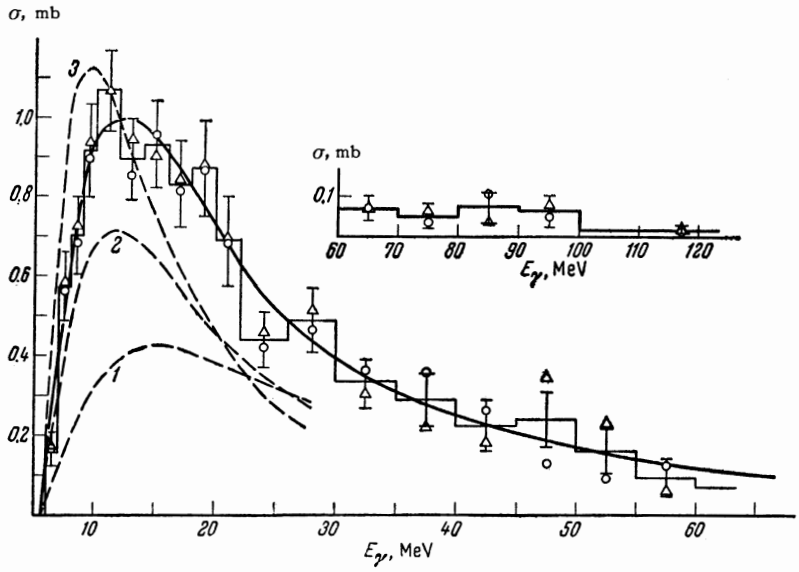

FIG. 4. Cross section for $He^3(\gamma, p)D^2$. o – from proton tracks; △ – from deuteron tracks.

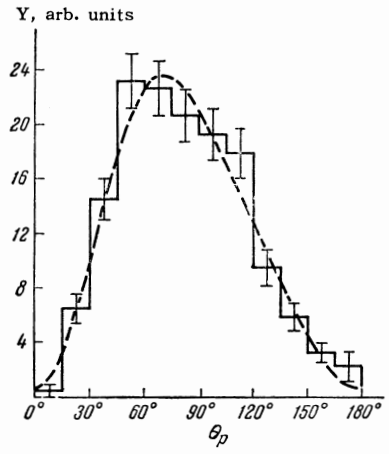

FIG. 5. Angular distribution of protons from the reaction $He^3(\gamma, p)D^2$ in the c.m. system. Dashed curve – distribution according to (5) with $\beta = 0.66 \pm 0.10$, $\gamma = 0.46 \pm 0.10$, and $\delta = 0.03 \pm 0.01$. Y is the yield per unit solid angle; E_γ = 6–170 MeV.

C. Angular distributions of protons from $He^3(\gamma, p)D^2$. Figure 5 shows the c.m.s. angular distribution of protons from (1). This angular distribution exhibits little energy dependence and has the form

$$f(\theta) \sim \sin^2\theta + \beta \sin^2\theta \cos\theta + \gamma \sin^2\theta \cos^2\theta + \delta \qquad (5)$$

The asymmetry of the angular distribution, with its maximum shifted forward to ~70–75°, begins to appear at low photon energies and is almost constant with increasing energy.

4. DISCUSSION OF RESULTS

The dashed curves in Fig. 4 represent the theoretical cross sections for electric-dipole two-body photodisintegration of H^3 [the reaction $H^3(\gamma, n)D^2$] calculated in [10]. Because of the charge independence of nuclear forces the cross sections for $H^3(\gamma, n)D^2$ and (1) should be identical except near threshold, where the Coulomb barrier for protons somewhat reduces the cross section for (1). In [10] the H^3 nucleus is described by Irving's two-body exponential function

$$\psi \approx \exp\left\{-\mu\left(\sum_{i>j} r_{ij}^2\right)^{1/2}\right\} \Big/ \left(\sum_{i>j} r_{ij}^2\right)^{1/2},$$

where r_{ij} is the distance between the i-th and j-th nucleons, and μ is a nuclear size parameter. These functions were selected only on the basis of their integrability and satisfactory asymptotic behavior. The parameter μ was selected by means of variational calculations of the H^3 binding energy and He^3 Coulomb energy. No account was taken of particle interaction in the final state.

The values of the parameter $1/\mu$ corresponding to the theoretical curves in Fig. 4 are given in the accompanying table, which also gives the rms radius $\langle R^2\rangle^{1/2}$ of the charge distribution in H^3 (He^3) calculated for point nucleons, as well as the binding energy E_b of H^3 and the Coulomb energy E_c for He^3 calculated with these wave functions. The last column of the table gives the ratio of the experimental and theoretical cross sections for (1) at its maximum.

	$1/\mu$, F	$\langle R^2\rangle^{1/2}$, F	E_b, MeV	E_c, MeV	$\frac{\sigma^{exp}_{max}}{\sigma^{theor}_{max}}$
Curve 1	2.0	1.48	7.1		2.5
Curve 2	2.5	1.85	6.3	0.8	1.4
Curve 3	3.0	2.22	5.0		1.0

Curve 1 was calculated for $1/\mu = 2.0$ F, leading to the best variational value of the binding energy of H^3, $E_b = 7.1$ MeV, for a central two-body Yukawa potential (the experimental binding energy of He^3 being $E_b^{exp} = 8.49$ MeV). This curve represents satisfactorily the position of the cross-section maximum, but gives a value of the cross section that is smaller than the experimental value by a factor of 2.5.

Curve 2 was calculated for $1/\mu = 2.5$ F, leading to the best variational value of the Coulomb energy of He^3, $E_c = 0.8$ MeV (compared with $E_c^{exp} = 0.764$ MeV). However, for this value of the parameter we have for the binding energy of H^3, $E_b = 6.3$ MeV, which is considerably below the experimental value. Curve 2 represents satisfactorily the position of the maximum and the shape of the cross-section curve, but gives a value of the cross section that is smaller than the observed value by a factor of almost 1.5.

Curve 3 was calculated for $1/\mu = 3.0$ F. In this case the binding energy obtained for H^3 was too low: $E_b = 5$ MeV. Curve 3 represents correctly the maximum cross section, but its shape differs greatly from the experimental curve.

The sum rules for electric dipole absorption are known to permit calculation of the integrated absorption cross section:

$$(\sigma_0)_{E1} = \int_0^\infty \sigma_{E1}(w)\, dw$$

and the quantity

$$(\sigma_{-1})_{E1} = \int_0^\infty \sigma_{E1}(w)\, \frac{dw}{w},$$

where $\sigma_{E1}(w)$ is the cross section for electric dipole absorption at the energy w. According to [11] we have

$$(\sigma_{-1})_{E1}=\frac{4\pi^2}{3}\left(\frac{e^2}{\hbar c}\right)\frac{N^2Z^2}{A^2}\langle R_{pn}^2\rangle,$$

where $\langle R_{pn}^2\rangle$ is the mean square distance between the centers of mass of the proton and neutron distributions in the nucleus. Foldy [12] has shown that if the ground-state wave function is symmetric in the spatial coordinates of all nucleons, we have

$$\langle R_{pn}^2\rangle=\frac{A^2}{ZN(A-1)}\langle R^2\rangle=\frac{A^2}{ZN(A-1)}(\langle R_c^2\rangle-\langle R_p^2\rangle),$$

where $\langle R^2\rangle^{1/2}$ is the rms radius of nuclear charge in the nucleus for point nucleons, $\langle R_c^2\rangle^{1/2}$ is the rms radius of nuclear charge distribution for finite nucleons, and $\langle R_p^2\rangle^{1/2}$ is the rms radius of proton charge distribution.

Thus, if the ground-state wave function is symmetric in the spatial coordinates of the nucleons, we have

$$(\sigma_{-1})_{E1}=\frac{4}{3}\pi^2\left(\frac{e^2}{\hbar c}\right)\frac{NZ}{A-1}[\langle R_c^2\rangle-\langle R_p^2\rangle],$$

so that by measuring $(\sigma_{-1})_{E1}$ we can determine the rms nuclear charge radius $\langle R_c^2\rangle^{1/2}$.

In order to determine σ_{-1} for He^3 we made use of the fact that the yields of (1) and (2) are identical:

$$\int_0^{170}\sigma_{\gamma p}(w)\,\eta(w)\,dw=\int_0^{170}\sigma_{\gamma n}(w)\,\eta(w)\,dw.$$

Since the bremsstrahlung spectrum $\eta(w)$ is close to $1/w$, we conclude from the equal yields of (1) and (2) that

$$\int_0^{170}\sigma_{\gamma p}\frac{dw}{w}=\int_0^{170}\sigma_{\gamma n}\frac{dw}{w}.$$

It follows that

$$\sigma_{-1}=2\int_0^{170}\sigma_{\gamma p}(w)\frac{dw}{w}=2(\sigma_{-1})_{\gamma p}.$$

The value of $(\sigma_{-1})_{\gamma p}$ was obtained from the cross section for (1):

$$(\sigma_{-1})_{\gamma p}=1.34\pm0.05\ \text{mb}.$$

It follows from an analysis of the angular distributions that the contribution of E2 absorption to $(\sigma_{-1})_{\gamma p}$ is 8.4 ± 2%. If the contribution of E2 absorption to $(\sigma_{-1})_{\gamma n}$ is taken to be the same, we have

$$(\sigma_{-1})_{E1}=2.45\pm0.14\ \text{mb}$$

with only the statistical errors indicated.

The last quantity given above considerably exceeds its theoretical value, $(\sigma_{-1})_{E1}$ = 1.32 mb, calculated in [13] using a two-body spin-dependent central Yukawa potential and the Irving wave function with a parameter chosen to make the binding energy agree with experiment. In later work [14, 15,17] the calculations of $(\sigma_{-1})_{E1}$ for three-particle nuclei employed different potentials. Thus the authors of [14,15] used the spin-dependent central potential of Kikuta et al., [16] containing a hard core, which enhanced the theoretical values of $(\sigma_{-1})_{E1}$ until they were close to the experimental value (σ_{-1} = 2.85 mb in [14] [2)] and σ_{-1} = 2.32 mb in [15]). In [17] $(\sigma_{-1})_{E1}$ was calculated using a potential containing a hard core along with tensor forces, with the result $(\sigma_{-1})_{E1}$ = 2.36 mb. However, it was here noted that $(\sigma_{-1})_{E1}$ can be derived without using a hard-core potential. For example, calculations based on the potential of Hu and Massey [18] yielded $(\sigma_{-1})_{E1}$ = 2.40 mb.

From the experimental value of $(\sigma_{-1})_{E1}$ we calculated the rms radius of charge distribution in He^3 (for point nucleons):

$$\langle R^2\rangle^{1/2}=1.60\pm0.07\ \text{F}.$$

If, following [19], we assume $\langle R_p^2\rangle^{1/2}$ = 0.805 ± 0.011 F the rms charge radius in He^3 for finite protons becomes

$$\langle R_c^2\rangle^{1/2}=1.79\pm0.07\,\text{F}.$$

Collard and Hofstadter [20] found from high-energy electron scattering that the rms charge radius in He^3 is $\langle R_c^2\rangle^{1/2}$ = 1.85 ± 0.18 F if the charge distribution is Gaussian, or $\langle R_c^2\rangle^{1/2}$ = 2.05 ± 0.2 F for an exponential charge distribution. It follows from this work that the exponential distribution is in better agreement with the dependence of the charge form factor on transferred momentum. The large experimental errors still prevent us from determining the agreement or disagreement between the values of $\langle R_c^2\rangle^{1/2}$ obtained for He^3 from electron scattering and the nuclear photoeffect. Taking for $\langle R_c^2\rangle^{1/2}$ its most reliable value obtained from electron scattering experiments, $\langle R_c^2\rangle^{1/2}$ = 2.05 F, the disagreement with our present work can apparently be accounted for by the incomplete spatial symmetry of the He^3 nucleus. [21]

We now return to the theoretical cross section for the reaction (1). The table gives the rms charge distribution radii in He^3 for point nucleons, calculated with the same Irving wave functions that were used in [10] to calculate the cross section for (1). The table shows that the exponential wave function corresponding to the correct binding energy of H^3 ($1/\mu$ = 2.0 F) leads to a low cross section for

---

[2)] An error in [14] was pointed out in [17]. Removal of this error increases σ_{-1} to 2.85 mb, instead of 2.72 mb.

(1) and to a radius of He^3 that is smaller than our experimental result. On the other hand, the exponential wave function corresponding to the correct Coulomb energy, ($1/\mu = 2.5$ F) exaggerates the radius of He^3, although the theoretical cross section remains, as previously, considerably smaller than the experimental value. Thus the theoretical curve of Gunn and Irving corresponding to the experimental radius of He^3 lies between curves 1 and 2 in Fig. 4 and is located considerably below the experimental points.

Fetisov,[15] using a wave function of H^3 with a solid nucleonic core[16] and parameters yielding the satisfactory values $E_C \sim 0.75$ MeV and $\langle R^2\rangle^{1/2}_{He^3} = 1.68$ F [$(\sigma_{-1})_{E1} = 2.7$ mb], calculated the cross section for (1) while neglecting particle interaction in the final state. In this case the experimental cross-section curve practically coincides with curve 2 of Fig. 4, thus lying considerably below the experimental points. Therefore the introduction of a repulsive core does not greatly affect the cross section if the wave-function parameters are selected to yield a given nuclear radius.

Therefore, theory and experiment disagree strongly at the present time; the theory explains satisfactorily the experimental integrated cross section and predicts correctly the combined yield of two-particle and three-particle disintegrations of He^3, but cannot account for the observed ratios between the cross sections for these channels. The similar situation in the case of He^4 should be noted; according to the theory in [10] the integrated cross section for the total photodisintegration of He^4 should be about 1.5 times greater than the cross section for two-particle photodisintegration. From [22] it follows that in actuality the cross section for the first process is only 2% of that for the second process. A possible explanation lies in the fact that the theoretical calculation neglected particle interaction in the final state, leading in the case of He^3 to a reduced cross section for the three-particle channel and to an enhanced cross section for the two-particle channel. We cannot, however, exclude the possibility that the discrepancy between theory and experiment results from the existence of many-body nuclear forces.

The integrated cross section for (1) was

$$(\sigma_0)_{\gamma p} = \int_0^{170} \sigma_{\gamma p}(w)\,dw = 26.5 \pm 1.3 \text{ MeV-mb}.$$

($\sigma_0 = 26.0 \pm 1.3$ MeV-mb from proton track measurements, and $\sigma_0 = 27.1 \pm 1.3$ MeV-mb from deuteron track measurements). If again, based on the equal yields of reactions (1) and (2), it is assumed that the integrated cross sections for these reactions will also not differ greatly, the integrated cross section for photon absorption by He^3 will be of the order of magnitude $\sigma_0 \sim 53$ MeV-mb. The theoretical integrated cross section for electric dipole absorption $(\sigma_0)_{E1}$ calculated in [13,14,17] by means of sum rules, lies in the range 51—65 MeV-mb, depending on the form of the potential and type of exchange-force mixture that were used, i.e., in good agreement with experiment. This circumstance, as well as the character of the observed angular distribution of protons in (1), furnishes evidence that the electric dipole absorption plays a fundamental role in the nuclear photoeffect in He^3.

In conclusion we wish to thank V. E. Yakushkin for his great labor in designing and preparing the apparatus, A. M. Ivanov and K. G. Kuvatov for assistance in preparing and adjusting the apparatus, V. A. Dubrovina, A. I. Orlova, V. A. Osipova, and G. G. Taran for experimental assistance, V. S. Silaeva and M. S. Starichenko for assistance in processing the results, V. N. Fetisov for discussion of the results, and T. Kruglova for electronic computer calculations.

Addendum (February 27, 1964). We have now determined $(\sigma_0)_{\gamma n}$ and $(\sigma_{-1})_{\gamma n}$ directly from experimental data for reaction (2):

$$(\sigma_0)_{\gamma n} = 43.6 \pm 2.7 \text{ MeV} \cdot \text{mb}$$
$$(\sigma_{-1})_{\gamma n} = 1.42 \pm 0.07 \text{ mb}$$

Accordingly, we have the improved cross sections and radii

$$\sigma_0 = 70 \pm 3 \text{ MeV} \cdot \text{mb}, \qquad \sigma_{-1} = 2.76 \pm 0.08 \text{ mb}.$$
$$\langle R^2\rangle^{1/2} = 1.62 \pm 0.06 \text{ F}, \qquad \langle R_c^2\rangle^{1/2} = 1.81 \pm 0.06 \text{ F}.$$
$$(\sigma_{-1})_{E1} = 2.53 \pm 0.12 \text{ mb}.$$

[1] L. Cranberg, Bull. Am. Phys. Soc. **3**, 173 (1958).

[2] G. M. Griffiths and J. B. Warren, Proc. Phys. Soc. (London) **68**, 781 (1955).

[3] Griffiths, Larson, and Robertson, Can. J. Phys. **40**, 402 (1962).

[4] A. N. Gorbunov and A. T. Varfolomeev, Phys. Letters **5**, 149 (1963).

[5] R. Wilson, Nuclear Instr. **1**, 101 (1957).

[6] Barber, George, and Reagan, Phys. Rev. **98**, 73 (1955).

[7] G. G. Taran and A. N. Gorbunov, JETP **46**, 1492 (1964), Soviet Phys. JETP **19**, 1010 (1964).

[8] A. N. Gorbunov and V. A. Osipova, JETP **43**, 40 (1962), Soviet Phys. JETP **16**, 27 (1963).

[9] Davies, Bethe, and Maximon, Phys. Rev. **93**, 788 (1954).

[10] J. C. Gunn and J. Irving, Phil. Mag. **42**, 1353 (1951).
[11] J. S. Levinger and H. A. Bethe, Phys. Rev. **78**, 115 (1950).
[12] L. L. Foldy, Phys. Rev. **107**, 1303 (1957).
[13] M. L. Rustgi, Phys. Rev. **106**, 1256 (1957).
[14] Mathur, Mukherjee, and Rustgi, Phys. Rev. **127**, 1663 (1962).
[15] V. N. Fetisov, JETP **46**, 1395 (1964), Soviet Phys. JETP **19**, 943 (1964).
[16] Kikuta, Morita, and Yamada, Progr. Theoret. Phys. (Kyoto) **15**, 222 (1956).
[17] P. O. Davey and H. S. Valk, Phys. Letters **7**, 155 (1963).
[18] T. Hu and H. S. W. Massey, Proc. Phys. Sov. (London) **A196**, 135 (1949).
[19] Hand, Miller, and Wilson, Revs. Modern Phys. **35**, 335 (1963).
[20] H. Collard and R. Hofstadter, Phys. Rev. **131**, 416 (1963).
[21] P. O. Davey and H. S. Valk, Phys. Letters **7**, 335 (1963).
[22] A. N. Gorbunov and V. M. Spiridonov, JETP **33**, 21 (1957), Soviet Phys. JETP **6**, 16 (1958).

Translated by I. Emin
7